Dalton Transactions

PAPER

View Article Online
View Journal | View Issue



Cite this: *Dalton Trans.*, 2018, **47**, 1566

# Steric control in the metal–ligand electron transfer of iminopyridine–ytterbocene complexes†

Alexander A. Trifonov, *[a,b] Tatyana V. Mahrova,[a] Lapo Luconi,[c] Giuliano Giambastiani, *[c,d] Dmitry M. Lyubov,[a] Anton V. Cherkasov,[a] Lorenzo Sorace, *[e] Elisa Louyriac,[f] Laurent Maron*[f] and Konstantin A. Lyssenko[b]

A systematic study of reactions between $Cp^*_2Yb(THF)$ ($Cp^* = \eta^5$-$C_5Me_5$, **1**) and iminopyridine ligands (IPy = 2,6-$^iPr_2C_6H_3N{=}CH(C_5H_3N$-R), R = H (**2a**), 6-$C_4H_3O$ (**2b**), 6-$C_4H_3S$ (**2c**), 6-$C_6H_5$ (**2d**)) featuring similar electron accepting properties but variable denticity and steric demand, has provided a new example of steric control on the redox chemistry of ytterbocenes. The reaction of the unsubstituted IPy **2a** with **1**, either in THF or toluene, gives rise to the paramagnetic species $Cp^*_2Yb^{III}(IPy)^{\bullet-}$ (**3a**) as a result of a formal one-electron oxidation of the $Yb^{II}$ ion along with IPy reduction to a radical-anionic state. The reactions of **1** with substituted iminopyridines **2b–d**, bearing aryl or hetero-aryl dangling arms on the 6 position of the pyridine ring occur in a non-coordinating solvent (toluene) only and afford coordination compounds of a formally divalent ytterbium ion, coordinated by neutral IPy ligands $Cp^*_2Yb^{II}(IPy)^0$ (**3b–d**). The X-ray diffraction studies revealed that **2a–c** act as bidentate ligands; while the radical-anionic IPy in **3a** chelates the $Yb^{III}$ ion with both nitrogens, neutral IPy ligands in **3b** and **3c** participate in the metal coordination sphere through the pyridine nitrogen and O or S atoms from the furan or thiophene moieties, respectively. Finally, in complex **3d** the neutral IPy ligand formally adopts a monodentate coordination mode. However, an agostic interaction between the $Yb^{II}$ ion and an *ortho* C–H bond of the phenyl ring has been detected. Imino-nitrogens in **3b–d** are not involved in the metal coordination. Variable temperature magnetic measurements on **3a** are consistent with a multiconfigurational ground state of the Yb ion and suggest that the largest contribution arises from the $4f^{13}$-radical configuration. For complexes **3b** and **3c** the data of magnetic measurements are indicative of a $Yb^{II}$-closed shell ligand electronic distribution. Complex **3d** is characterized by a complex magnetic behavior which does not allow for an unambiguous estimation of its electronic structure. The results are rationalized using DFT and CSSCF calculations. Unlike diazabutadiene analogues, **3a** does not undergo a solvent mediated metal–ligand electron transfer and remains paramagnetic in THF solution. On the other hand, complexes **3b–d** readily react with THF to afford **1** and free IPy **2b–d**.

Received 14th November 2017,
Accepted 20th December 2017

DOI: 10.1039/c7dt04299j

rsc.li/dalton



## Introduction

Since the pioneering studies of Cloke and Edelmann[1] in the early 1980s who introduced diimines in organolanthanide chemistry, this field of coordination chemistry has received a large boost due to the diversity of coordination modes offered by this class of ligands along with their intriguing redox properties.[2] The idea to combine redox active diimine ligands[3] and ytterbium ions possessing two stable oxidation states[4] has proven to be particularly fruitful[5] thus leading to the discovery of a series of challenging phenomena such as solvent mediated redox transformations,[5c,6] sterically induced reduction[7] and redox isomerism.[7,8] The course of the reactions between ytterbocenes and diimine ligands has been found to be affected by a number of factors. Depending on the nature of

[a]*G. A. Razuvaev Institute of Organometallic Chemistry of Russian Academy of Sciences, Tropinina str. 49, 603950 Nizhny Novgorod, GSP-445, Russia. E-mail: trif@iomc.ras.ru*
[b]*A. N. Nesmeyanov Institute of Organoelement Compounds of Russian Academy of Sciences, 28 Vavilova str., 119991 Moscow, GSP-1, Russia*
[c]*Istituto di ChimicadeiCompostiOrganometallici (ICCOM - CNR), Via Madonna del Piano 10, 50019 Sesto Fiorentino, Italy*
[d]*Kazan Federal University, 420008 Kazan, Russian Federation*
[e]*Dipartimento di Chimica "U. Schiff" and UdR INSTM, Università di Firenze, 50019 Sesto Fiorentino, Italy*
[f]*Université de Toulouse, INSA, UPS, CNRS-UMR5215, LPCNO Avenue de Rangueil 135, 31077 Toulouse, France*

†Electronic supplementary information (ESI) available. CCDC 1552992–1552995. For ESI and crystallographic data in CIF or other electronic format see DOI: 10.1039/c7dt04299j

cyclopentadienyl-type ligands (Cp = cyclopentadienyl, indenyl, fluorenyl), their binding mode to the $Yb^{II}$ ion (propensity to Cp-haptotropic rearrangements),[9] and the steric demand of a diimine ligand, the reactions of ytterbocenes with diimines can result in either $Yb^{II}/Yb^{III}$ oxidation,[6,10] formation of new C–C bonds[11] or C–H bond activation at the diamine skeleton.[12] The one-electron oxidation of ytterbocenes by diazabutadienes proved to be a sterically governed redox process.[13] Depending on the steric hindrance of the ytterbium coordination sphere, $Yb^{III}$ complexes containing either radical-anionic diazabutadiene or covalently bonded imino-amido ligands can be formed.

Iminopyridine (IPy) ligands belong to the same family of redox active diimine systems but their coordination chemistry with lanthanide ions still remains only moderately investigated[14] and certainly much less studied than that of their saturated aminopyridine (APy) counterparts.[14]

In recent years our group has shown how the reaction of variably hindered ytterbocenes $[L]_2Yb(THF)_n$ (L = $\eta^5$-$C_{13}H_9$ (fluorenyl); $\eta^5$-$C_9H_7$ (indenyl); $\eta^5$-$C_5Me_5$; $\eta^5$-$C_5H_4Me$) with a bidentate IPy ligand [2,6-$^i$Pr$_2$C$_6$H$_3$N=CH(C$_5$H$_4$N)] can lead to a dramatic rearrangement of the metal coordination sphere through unusual reactivity paths together with a permanent change of the ion oxidation state (Fig. 1).

The $Yb^{II}$ bis(fluorenyl) complex $(\eta^5\text{-}C_{13}H_9)_2Yb(THF)_2$ in the presence of an excess of IPy, proceeds through the complete oxidative cleavage of the two $\eta^5$-coordinated fragments, affording the paramagnetic $Yb^{III}$ species coordinated by three iminopyridyl radical-anions (**I**).[11b] Similarly, the $Yb^{II}$ bis(indenyl) complex $(\eta^5\text{-}C_9H_7)_2Yb(THF)_2$ undergoes an unusual N=C bond insertion into a formal $\eta^1$-Yb–$C_9H_7$ bond thus leading to the half-sandwich and oxidized compound (**II**).[11b] When bis(cyclopentadienyl) ytterbium complexes $Cp_2Yb(THF)_n$ (Cp = $\eta^5$-$C_5Me_5$, $\eta^5$-$C_5H_4Me$) are reacted with two equivalents of the same IPy a similar oxidative cleavage at one Yb–Cp bond takes place and $Yb^{III}$ species (**III**) coordinated by two iminopyridyl radical-anions are formed.[11a,15] For all these reactions, steric factors and the inherent tendency of the $\eta^5$-coordinated ligands to undergo haptotropic rearrangement are claimed to play a fundamental role in the whole transformation.

Despite the intriguing reactivity issues observed in the reaction of $(\eta^5\text{-}C_9H_7)_2Yb(THF)_2$ with the bidentate IPy ligand, 6-(hetero)aryl substituted analogues [2,6-$^i$Pr$_2$(C$_6$H$_3$)N=CH(C$_5$H$_3$N)-6-R′ (R′ = 2-furyl, 2-thiophenyl, phenyl)] behave unexpectedly as neutral ($\kappa^2$-or $\kappa^3$-coordinated) systems by replacing THF molecules from the metal coordination sphere, without affecting the metal oxidation state of the targeted coordinative compounds (**IV**).[16] The reason for the inhibition of metal-to-ligand electron transfer in the latter compounds is likely due to the lack of convergence between the ytterbium center and the bulkier substituted IPy ligands as a consequence of a metal ion size decrease in the case of a $Yb^{II}/Yb^{III}$ oxidation.[17] To gain additional insight into the steric regulation of these redox processes and to clarify the role of the steric and electronic properties of ligands bound to the ytterbium ion, hereafter we performed the study of the model ytterbocene complexes $Cp^*_2Yb(THF)$ ($Cp^*$ = $\eta^5$-$C_5Me_5$) with unsubstituted and 6-(hetero)aryl-substituted iminopyridine ligands. A series of di- and trivalent ytterbium complexes coordinated by neutral or radical anionic ligands have been synthesized and fully characterized.

## Experimental section

### General considerations and material characterization

All experiments were performed under an inert atmosphere, using standard Schlenk-tube and glove-box techniques. After drying over KOH, THF was purified by distillation from sodium/benzophenone ketyl and hexane and toluene were dried by distillation from sodium/triglyme benzophenone ketyl prior to use. $(\eta^5\text{-}C_5Me_5)_2Yb(THF)$,[18] IPy **2a**[19] and IPy **2b–d**[13,16,20] were prepared according to literature procedures. Unless otherwise stated, all commercially available chemicals were used as provided from commercial supplies. $^1$H and $^{13}$C $\{^1H\}$ NMR spectra were obtained on either a Bruker Avance-II 400 MHz NMR spectrometer or a Bruker DPX 200 MHz NMR spectrometer. Chemical shifts ($\delta$) are reported in ppm relative to tetramethylsilane (TMS), referenced to the chemical shifts of residual solvent resonances ($^1$H and $^{13}$C). IR spectra were recorded as Nujol mulls on a Bruker-Vertex 70 spectrophotometer. The N, C, and H elemental analyses were carried out in the microanalytical laboratory of the IOMC by means of a Carlo Erba Model 1106 elemental analyzer with an accepted tolerance of 0.4 unit on carbon (C), hydrogen (H), and nitrogen (N). Lanthanide metal analysis was carried out by complexometric titration.[21]

### General procedure for the synthesis of 3a–d

In a typical procedure, a toluene solution (20 mL) of $(\eta^5\text{-}C_5Me_5)_2Yb(THF)$ (**1**) (0.50 g, 0.97 mmol) was treated drop-

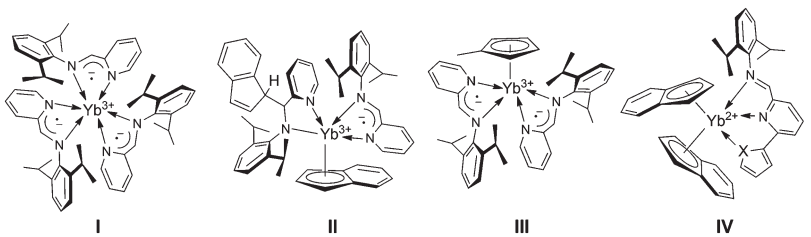


Fig. 1 Representative examples of recently prepared Yb-complexes with IPy ligands.

wise with a toluene solution (10 mL) of the appropriate ligand (**2a–d**) (0.97 mmol) and the reaction mixtures were maintained under stirring at 50 °C for the expected reaction times (24 h for **3a** and **3c**; 12 h for **3b**; 28 h for **3d**). For **3a**, after removing volatiles under vacuum, the brownish-black solid was re-dissolved in 20 mL of nonane and the solution was cooled down to −20 °C to give brownish-black crystals of the complex in 76% yield. For **3b–d**, brownish-black crystals were obtained directly from slow concentration of the toluene mixtures at room temperature in 70, 48 and 32% yield, respectively. Characterization data for $(C_5Me_5)_2Yb[\kappa^2\text{–}2,6\text{-}^iPr_2(C_6H_3)NCH(C_5H_4N)]^{\bullet-}$ (**3a**): elemental analysis calcd (%) for $C_{38}H_{48}N_2Yb$: C, 64.29; H, 7.38; N, 3.95; Yb, 24.38; found (%): C, 63.88; H, 7.01; N, 4.17; Yb, 24.56. IR (Nujol, KBr) $\nu$/cm$^{-1}$: 1575 (s), 1380 (s), 1265 (s), 1235 (s), 1155 (s), 1100 (m), 995 (s), 895 (s), 850 (m), 820 (s), 725 (s). $^1$H NMR (200 MHz, $C_6D_6$, 293 K, sw = 200 ppm): −70.3 (s), −32.4 (s), −16.3 (br s), −12.1 (br s), −7.9 (br s), −7.4 (s), −6.11 (s), 3.41 (s, $CH_3$ Cp*), 11.8 (s), 18.7 (s), 23.2 (s), 26.4 (s), 33.2 (s), 43.2 (s), 80.8 (s) ppm. Characterization data for $(C_5Me_5)_2Yb[\kappa^2\text{-}2,6\text{-}^iPr_2C_6H_3NCH(C_5H_4N)\text{-}6\text{-}(C_4H_3O)]$ (**3b**): elemental analysis calcd (%) for $C_{42}H_{54}N_2OYb$: C, 65.01; H, 7.01; N, 3.61; Yb, 22.30; found (%): C, 65.36; H, 7.12; N, 3.31; Yb, 22.04. IR (Nujol, KBr), $\nu$/cm$^{-1}$:1635 (s), 1560 (s), 1315 (m), 1270 (s), 1160 (m), 1020, 810 (s), 755 (m). $^1$H NMR (200 MHz, $C_6D_6$, 293 K): 1.33 (d, $^3J_{HH}$ = 6.5 Hz, 12H, $CH_3{}^iPr$), 1.92 (s, 30H, $CH_3$ Cp*), 3.41 (sept, $^3J_{HH}$ = 6.5 Hz, 2H, CH $^i$Pr), 6.01 (br s, 1H, N=CH), 6.47 (br s, 1H, CH Ar), 6.69 (br d, $^3J_{HH}$ = 7.5 Hz, 1H, CH Ar), 7.20 (m, 3H, CH Ar), 7.83 (m, 2H, CH Ar), 8.14 (br d, $^3J_{HH}$ = 7.5 Hz, 1H, CH Ar), 8.59 (br s, 1H, CH Ar) ppm. $^{13}C\{^1H\}$ NMR (50 MHz, $C_6D_6$, 293 K): 10.7 (s, $CH_3$, $C_5Me_5$), 22.2 (s, $CH_3{}^iPr$), 28.4 (s, CH $^i$Pr), 110.6 (s, CH Ar), 111.3 (s, C $C_5Me_5$), 113.3 (s, CH Ar), 122.7 (s, CH Ar), 123.2 (s, CH Ar), 123.7 (s, CH Ar), 125.4 (s, C Ar), 134.9 (s, CH Ar), 136.1 (s, CH Ar), 137.2 (s, C Ar), 137.6 (s, CH Ar), 143.8 (s, C Ar), 148.5 (s, C Ar), 152.3 (s, C Ar), 158.4 (s, CH=N) ppm. Characterization data for $(C_5Me_5)_2Yb[\kappa^2\text{-}2,6\text{-}^iPr_2C_6H_3NCH(C_5H_4N)\text{-}6\text{-}(C_4H_3S)]$ (**3c**): elemental analysis calcd (%) for $C_{42}H_{54}N_2SYb$: C, 63.69; H, 6.87; N, 3.54; Yb, 21.85; found (%): C, 63.36; H, 7.12; N, 3.31; Yb, 22.14. IR (Nujol, KBr), $\nu$/cm$^{-1}$: 1685 (m), 1645 (m), 1570 (s), 1380 (s), 1320 (w), 1255 (w), 1180 (m), 1080 (m), 930 (w), 850 (m), 715 (m). $^1$H NMR (200 MHz, $C_6D_6$, 293 K): $^1$H NMR (200 MHz, $C_6D_6$, 293 K): 1.77 (d, $^3J_{HH}$ = 7.0 Hz, 12H, $CH_3{}^iPr$), 2.11 (br s, 30H, $CH_3$ Cp*), 3.42 (br sept, $^3J_{HH}$ = 7.0 Hz, 2H, CH $^i$Pr), 6.51 (d, $^3J_{HH}$ = 7.6 Hz, 1H, CH Ar), 6.73 (m, 2H, N=CH and CH Ar), 6.97 (m, 4H, CH Ar), 7.33 (br s, 1H, CH Ar), 7.55 (br s, 1H, CH Ar), 7.79 (d, $^3J_{HH}$ = 7.6 Hz, 1H, CH Ar) ppm. Characterization data for $(C_5Me_5)_2Yb[\kappa^1\text{-}2,6\text{-}^iPr_2C_6H_3NCH(C_5H_4N)\text{-}6\text{-}Ph]$ (**3d**): elemental analysis calcd (%) for $C_{44}H_{56}N_2Yb$: C, 67.24; H, 7.18; N, 3.56; Yb, 22.02; found (%): C, 66.98; H, 7.12; N, 3.31; Yb, 22.14. IR (Nujol, KBr), $\nu$/cm$^{-1}$: 1645 (s), 1585 (s), 1320 (s), 1180 (m), 1029 (s), 820 (s), 740 (s), 725 (m). $^1$H NMR (200 MHz, $C_6D_6$, 293 K): 1.31 (d, $^3J_{HH}$ = 7.0 Hz, 6H, $CH_3{}^iPr$), 1.77 (d, $^3J_{HH}$ = 7.0 Hz, 6H, $CH_3{}^iPr$), 2.24 (br s, 30H, $CH_3$ Cp*), 3.39 (m, 1H, CH $^i$Pr), 3.65 (m, 1H, CH $^i$Pr), 6.07 (s, 1H, N=CH), 6.48–7.03 (complex m, 7H, CH Ar), 7.42 (m, 2H, CH Ar), 7.97 (m, 1H, CH Ar), 8.29 (m, 1H, CH Ar) ppm.

### Magnetic characterization

Magnetic measurements of crystalline samples of **3a–d** were carried out by using an MPMS-XL SQUID magnetometer in the temperature range of 1.8–300 K with an applied magnetic field of 1000 Oe (up to 40 K) and 10 000 Oe (from 40 K to 350 K), to avoid saturation effects. Samples were prepared in a glove box by wrapping them in Teflon and then loaded in the SQUID magnetometer in less than 30″. The susceptibility is evaluated in the low field limit as $\chi_m = M_m/H$. The raw data have been corrected for diamagnetic contribution of the sample holder, and the intrinsic diamagnetism of the sample, estimated by using Pascal's constant to obtain the paramagnetic susceptibility.

### X-ray crystallography

The X-ray data for **3a–d** were collected on Bruker Smart Apex (**3b**,**d**), Bruker D8 Quest (**3a**) and Agilent Xcalibur E (**3c**) diffractometers (MoK$_\alpha$-radiation, $\omega$-scans technique, $\lambda$ = 0.71073 Å, $T$ = 100(2) K) using SMART,[22] APEX2[23] and CrysAlis PRO[24] software packages. The structures were solved by direct and dual-space[25] methods and were refined by full-matrix least squares on $F^2$ for all data using SHELX.[25a] SADABS[26] and CrysAlis PRO were used to perform area-detector scaling and absorption corrections. All non-hydrogen atoms were found from Fourier syntheses of electron density and were refined anisotropically. Hydrogen atoms H(10A) in **3b,c** and H(3A) in **3d** also were found from Fourier syntheses of electron density and were refined isotropically. Other hydrogen atoms in **3a–d** were placed in calculated positions and were refined in the "riding" model with $U(H)_{iso}$ = 1.2 $U_{eq}$ of their parent atoms ($U(H)_{iso}$ = 1.5 $U_{eq}$ for methyl groups). 1552992 (**3a**), 1552993 (**3b**), 1552994 (**3c**), 1552995 (**3d**)† contain the supplementary crystallographic data for this paper. The crystallographic data and structure refinement details are given in Table S1.†

### Computational details

The calculations have been carried out with the Gaussian09 software[27] at the DFT level using the hybrid functional B3PW91.[28] Ytterbium atoms were treated with the small-core pseudopotential from the Stuttgart group,[29] that explicitly account for the 4f electrons. Oxygen, carbon and hydrogen atoms have been treated with the all electron 6-31G** Pople basis set.[30] The geometry optimization has been performed without any symmetry constraints taking the geometry obtained from the X-ray diffraction measurement of the product. Analytical calculations of the vibrational frequencies of the optimized geometry were done to confirm that it's a minimum. CASSCF calculations were also carried out based on the SCF orbitals obtained for the triplet state and the active space choice is detailed in the manuscript.

## Results and discussion

When a dark-red THF solution of Cp*$_2$Yb(THF) (**1**) is treated at room temperature with an equimolar amount of IPy ligand **2a**,

 

the colour of the reaction mixture changed rapidly to deep brown thus indicating that a reaction takes place. Following the process by $^1$H NMR (THF-$d_8$, 293 K) spectroscopy proved the rapid oxidation of the metal ion to Yb$^{III}$ and the subsequent formation of a paramagnetic species. This result contrasts with earlier observations dealing with the reactivity of ytterbocenes in the presence of *N*,*N*-disubstituted diazabutadienes[7] where only non-coordinating aromatic and aliphatic hydrocarbons[5,6,16] allowed the reaction to take place, whereas no interaction occurred in the presence of coordinating solvents (*i.e.* THF, py). Hereby, **2a** reacts with ytterbocene **1** in THF to give the paramagnetic complex $(C_5Me_5)_2Yb[\kappa^2$-2,6-$^i$Pr$_2$(C$_6$H$_3$)NCH(C$_5$H$_4$N)]$^{\bullet-}$ (**3a**) as a result of a formal one-electron oxidation of the metal ion and IPy ligand reduction to the radical-anionic state (Scheme 1). In the present case, THF-to-IPy ligand displacement at the ytterbium center is likely facilitated by the reduced steric hindrance of IPy[16] compared to the more commonly used and sterically demanding *N*,*N*-disubstituted diazabutadiene systems.[7]

**3a** was isolated in 76% yield as dark brown, air- and moisture-sensitive, microcrystals. Single crystals suitable for X-ray study were obtained from a concentrated toluene solution of the compound, cooled down to −20 °C for days. A perspective view of the **3a** structure is given in Fig. 2 along with a selection of the main

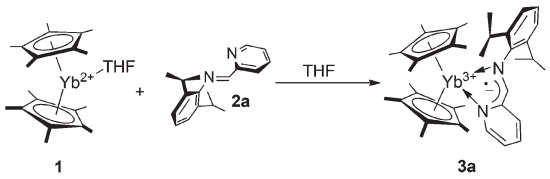


**Scheme 1** Reaction scheme for the generation of the paramagnetic species **3a**.

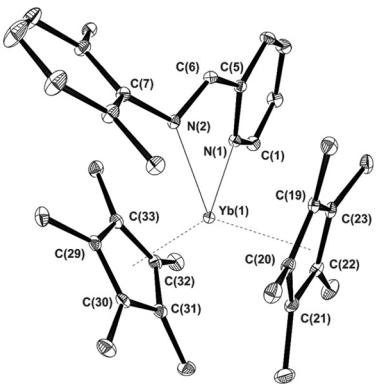


**Fig. 2** ORTEP diagram (30% probability thermal ellipsoids) of complex $(C_5Me_5)_2Yb[\kappa^2$-2,6-$^i$Pr$_2$(C$_6$H$_3$)NCH(C$_5$H$_4$N)]$^{\bullet-}$ (**3a**). Hydrogen atoms and Me-substituents at the $^i$Pr-groups are omitted for clarity. Selected bond distances (Å) and bond angles (°): Yb(1)–C(29) 2.601(2), Yb(1)–C(30) 2.618(2), Yb(1)–C(33) 2.624(2), Yb(1)–C(22) 2.660(2), Yb(1)–C(20) 2.662(2), Yb(1)–C(32) 2.665(2), Yb(1)–C(31) 2.672(2), Yb(1)–C(19) 2.670(2), Yb(1)–C(23) 2.668(2), Yb(1)–C(21) 2.671(2), Yb(1)–N(1) 2.325(2), Yb(1)–N(2) 2.385(2), N(2)–C(6) 1.348(3), C(5)–C(6) 1.408(3), N(1)–Yb(1)–N(2) 72.84(7), $Cp_{Centr}$–Yb–$Cp_{Centr}$ 132.9(2).

structural details [bond lengths (Å) and angles (°)]. The structure refinement data are given in Table S1 (see the ESI†).

The ytterbium ion is $\eta^5$-coordinated by two Cp* ligands together with the two nitrogen atoms from the IPy framework that formally increase the final complex coordination number to eight (assuming CN 3 assigned for the Cp ligand). The Yb–C bond lengths in **3a** [Yb–$C_{mean}$: 2.651(6) Å; Yb–$Cp_{centre}$: 2.345(2) Å] are shorter than those measured on both the IPy-free ytterbocene **1** (Yb–$C_{mean}$ 2.69 Å; Yb–$Cp_{centre}$: 2.41 Å)[31] and the diamagnetic eight-coordinated pyridine adduct $(Cp^*)_2Yb(Py)_2$ (Yb–$C_{mean}$ 2.74 Å).[32] On the other hand, they are in good accord with Yb–C bond distances measured in related eight-coordinated Yb$^{III}$ complexes of the state-of-the-art {*i.e.* ($\eta^5$-$C_5Me_4H)_2$YbI(THF) [Yb–$C_{mean}$ 2.60(4) Å],[33] ($\eta^5$-$C_5Me_4H)_2$Yb($\mu$-Cl)$_2$Li(THF)$_2$ [Yb–$C_{mean}$ 2.604(6) Å],[34] $(C_5Me_5)_2$YbF(THF) [Yb–$C_{mean}$ 2.628(5) Å][35] and $(C_5Me_5)_2$YbF(Et$_2$O) [Yb–$C_{mean}$ 2.631(8) Å]}.[35] The 5-membered YbNCCN metallacycle in **3a** is not planar and it forms a dihedral angle of 27.0(2)° between the planes defined by YbNN and NCCN atoms. Yb–N bond lengths [2.325(2), 2.385(2) Å] fall in a close range of those formerly reported for the related paramagnetic ytterbocene complexes coordinated by radical-anionic diazabutadiene ligands {*i.e.* ($\eta^5$-$C_5Me_5)_2$Yb$^{III}$(RNCHCHNR)$^{\bullet-}$ [R = $^t$Bu, Yb–N 2.358(3), 2.394(3) Å;[6a] R = *p*-tolyl, Yb–N 2.340(5), 2.368(5) Å;[5b] R = *p*-anisyl, Yb–N 2.339(7), 2.337(6) Å]}.[5b] Finally, bond distances within the NCCN fragment are markedly different from those typically measured for transition metal-coordinated[36] neutral IPy ligands [for **3a**: *d*(C=N) = 1.348(3) Å; *d*(C–C) = 1.408(3) Å]. For model transition metal compounds containing neutral IPy ligands: IPyM$^{II}$Cl$_2$ (M$^{II}$ = Pd,[36] Ni;[36b] IPy = **2a**): *d*(C=N) = 1.279(4)–1.278(3) Å; *d*(C–C) = 1.457(5)–1.463(4) Å]. All these data taken together largely support the hypothesis of a trivalent oxidation state for the ytterbium ion in **3a** as a result of one-electron metal oxidation along with a reduction of the coordinated IPy ligand to the state of a radical-anionic species.[11b,15,37] However, all our attempts to detect the paramagnetic radical-anionic iminopyridine ligand in **3a** (both in the solid state and in solution – hexane, toluene; 203–293 K) by the EPR technique failed. This outcome is in line with our previous studies where we demonstrated that Yb$^{III}$ complexes coordinated by paramagnetic radical-anionic diimino ligands are EPR-silent.[6,10] In addition, this behavior was not surprising at all given the fast electronic relaxation characterizing Yb$^{III}$ complexes and the even number of unpaired electrons of the resulting species.[38]

The temperature dependence of the magnetic moment and of the molar susceptibility of **3a** is reported in Fig. 3. A maximum in $\chi_M$ *vs.* *T* data is observed, together with the presence of an unavoidable paramagnetic impurity of Yb$^{III}$ coordinated to diamagnetic ligands, which is responsible for the paramagnetic tail observed at $T < 50$ K (Fig. 3A). By a fit of the low temperature region using a Curie law this is estimated to be 8.1%. This allowed correction of the data of Fig. 3A by following the procedure reported by Booth and co-workers.[39] The corrected curves shown in Fig. 3B present a maximum in $\chi_M$ at 170 K along with a temperature independent paramagnetism

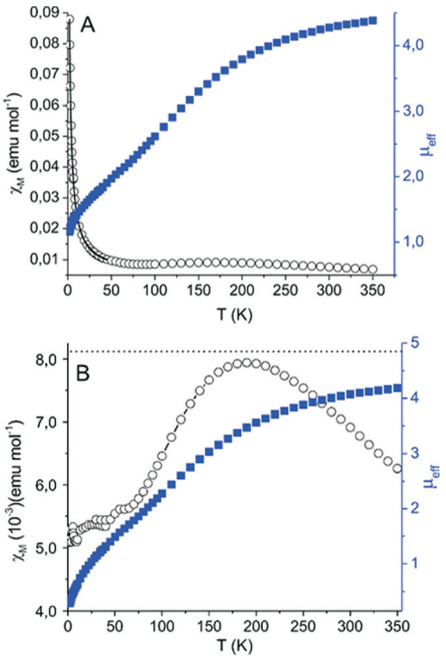


**Fig. 3** (A) $\mu_{eff}$ *vs. T* and $\chi_M$ *vs. T* curves of **3a** before correction for the paramagnetic impurity. The dotted line represents the fit to estimate the amount of paramagnetic $Yb^{III}$ impurity assuming a Curie–Weiss behavior; (B) $\mu_{eff}$ *vs. T* and $\chi_M$ *vs. T* curves of **3a** after correction for the paramagnetic impurity. The horizontal dashed line represents the $\mu_{eff}$ value expected at high temperature for a system formed by uncoupled $Yb^{III}$ and $S = 1/2$.

contribution of $5.4 \times 10^{-3}$ emu $mol^{-1}$. Both these values are consistent with a multiconfigurational ground state[39] and the observed $\mu_{eff}$ value at the highest measured temperature (4.19 at 350 K) suggests that the largest contribution is from the $4f^{13}$-radical configuration (expected $\mu_{eff}$ = 4.8 for uncoupled spins), in agreement with the results from the X-ray diffraction data.

The $^1$H NMR spectroscopy is a sensitive tool that allows for determining the magnetism of complexes in solution. The proton NMR spectrum can qualitatively indicate whether the complex is diamagnetic or paramagnetic. The $^1$H NMR spectrum of **3a** (benzene-$d_6$, 293 K) shows a set of broadened signals that are substantially shifted with respect to those of related diamagnetic species (Fig. S1, ESI†) thus giving an additional proof of its paramagnetic nature. The methyl protons of the $C_5Me_5$ ring appear as a slightly broadened singlet at 3.41 ppm, in good agreement with the chemical shifts measured for related paramagnetic species containing $Yb^{III}$ ions coordinated by radical-anionic bipyridine, phenanthroline or related ligands. The protons of the radical-anionic iminopyridine ligand give rise to a set of signals in a broad interval from −70 to 80 ppm.

Finally, the room-temperature electronic absorption spectra of **3a** (recorded in nonane), the radical-anionic potassium derivative $[2,6\text{-}^{i}Pr_2(C_6H_3)NCH(C_5H_4N)]^{\bullet-}K^+$ (recorded in THF) and of the neutral Ipy **2a** (recorded in hexane) were put at comparison for the sake of completeness. The spectra are shown in Fig. S3 (see the ESI†). The UV-Vis spectrum of **3a** shows two absorption bands at 355 and 455 nm, respectively. While the neutral IPy ligand **2a** displays a single absorbance at 340 nm, its potassium radical-anionic derivative $[2,6\text{-}^{i}Pr_2(C_6H_3)NCH(C_5H_4N)]^{\bullet-}K^+$ also displays two main absorbances at 355 and 525 nm, respectively. This comparative analysis is in line with the presence of a radical-anionic iminopyridine ligand in solution and corroborates with the NMR data on the paramagnetic nature of **3a**.

With the aim of gaining additional insight into the role of steric factors driving the metal-to-ligand electron transfer in the above-mentioned coordinative compounds, we studied the reaction of **1** in the presence of bulkier IPy ligands (**2b–d**), bearing coordinating or not-coordinating (hetero)aryl fragments attached to the six-position of the pyridine core (Scheme 2).

This systematic investigation takes advantage of the previous outcomes of our study of the coordination modes and electronic effects resulting from the reaction of the same class of IPy ligands with the bulkier bis(indenyl) ytterbium complex $(\eta^5\text{-}C_9H_7)_2Yb^{II}(THF)_2$.[16] In that case, the coordination of 6-(hetero)aryl-substituted IPy ligands occurred with the generation of diamagnetic species as a result of the simple replacement of the two coordinated THF molecules.

Unlike the above-mentioned reaction with the bidentate IPy **2a**, $Cp^*_2Yb(THF)$ (**1**) does not react in THF with the more sterically demanding ligands **2b–d**. This was preliminary confirmed by the absence of any appreciable color change in the solutions of **1** upon treatment with an equimolecular amount of **2b–d**. In addition, monitoring the reaction course over several hours by $^1$H NMR (THF-$d_8$, 293 K) spectroscopy has showed only signals from unreacted starting materials. On the contrary, the addition of **2a–d** to a toluene solution of **1** at room temperature (Scheme 2) resulted in the immediate change of the solution colour from dark-red to brownish-black. After slow concentration of each solution, brownish-black microcrystals of complexes $(C_5Me_5)_2Yb[\kappa^2\text{-}2,6\text{-}^{i}Pr_2C_6H_3NCH(C_5H_4N)\text{-}6\text{-}(C_4H_3O)]$ (**3b**), $(C_5Me_5)_2Yb[\kappa^2\text{-}2,6\text{-}^{i}Pr_2C_6H_3NCH(C_5H_4N)\text{-}6\text{-}(C_4H_3S)]$ (**3c**), $(C_5Me_5)_2Yb[\kappa^1\text{-}2,6\text{-}^{i}Pr_2C_6H_3NCH(C_5H_4N)\text{-}6\text{-}Ph]$ (**3d**) were obtained in 70, 48 and 32% isolated yields, respectively. Complexes **3b–d** were isolated as highly air-and moisture-sensitive solids showing moderate solubility in aromatic and aliphatic hydrocarbons thus hampering their full NMR characterization ($^{13}C\{^1H\}$ NMR spectra).

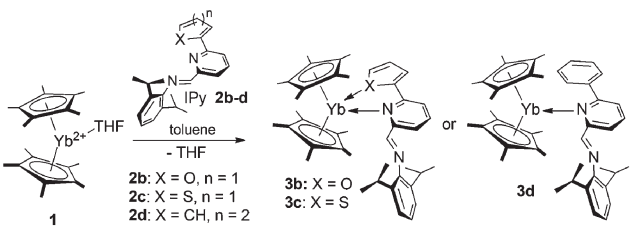


**Scheme 2** Reaction scheme for the generation of the coordination compounds **3b–d**.

Crystals suitable for single-crystal X-ray diffraction studies were grown by slow concentration of the respective toluene solutions at ambient temperature under a gentle stream of nitrogen. Complex **3b** crystallizes as a solvate with one molecule of toluene while crystals of **3c** and **3d** do not contain any crystallization solvent. ORTEP representations of the three crystal structures are given in Fig. 4–6 along with a selection of the main structural details [bond lengths (Å) and angles (°)]; Table S1† lists their main crystal data and structural refinement details.

At odds with previously reported bis(indenyl)ytterbium/IPy coordination derivatives[16] where ligands **2b** and **2c–d** behaved as tridentate and bidentate systems, respectively, the reaction of **1** with **2b–d** leads to complexes **3b–d** featuring different denticity of the coordinated IPys. As shown in Fig. 4 and 5, the potentially tridentate ligands **2b–c** coordinate the metal ion as bidentate ($\kappa^2$) systems involving donor atoms of both heterocycles thus resulting in a formal coordination number of eight for the ytterbium ion, whereas imino nitrogens point away from the metal coordination sphere. In the case of the bidentate ligand **2d**, only the pyridine core coordinates the ytterbium ion ($\kappa^1$) along with an agostic interaction at a C–H bond of the phenyl substituent [Yb(1)–C(3) = 2.969(3) Å, Yb(1)–H(3A) = 2.49(3) Å, Yb(1)–H(3A)–C(3) = 162.2(7)°]. Therefore, **2d** formally behaves as a monodentate ($\kappa^1$) system, again keeping away the imino nitrogen from the metal center as for previously described complexes **3b–c**. The increased steric demand of $\eta^5$-Cp* with respect to indenyl in the ytterbocene complex is largely responsible of the different IPy coordination mode around the metal ion. Although Yb–C bond distances in **3b–d** are reasonably longer than those measured in precursor **1** [$d$(Yb–C$_{mean}$) for **1**: 2.651(6) Å; for **3b**: 2.689(8) Å; for **3c**: 2.711(9) Å, for **3d**: 2.715(7) Å] as well as in the (Cp*)$_2$Yb(bipy) adduct from the literature[40] (Yb–C$_{mean}$: 2.62 Å), an appreciable shortening is measured with respect to another eight-coordinate ytterbocene/pyridine adduct of the state-of-the-art [$d$(Yb–C$_{mean}$) for (Cp*)$_2$Yb(Py)$_2$: 2.74 Å].[32] In spite of close stereo-electronic and redox properties of IPy ligands of this series (**2b–d**)[16] such a shortening effect is more evident in **3b** compared to the other related complexes **3c,d**. This trend is also observed for the Yb–N bond distances. Indeed, complex **3b** presents a Yb–N bond length [2.535(2) Å] that is noticeably shorter than that measured on the related compounds **3c,d** [**3c**: 2.623(2) Å; **3d**: 2.602(2) Å].

The magnetic properties of **3b–d** are outlined in Fig. 7 as $\mu_{eff}$ *vs. T*. For compounds **3b** and **3c** only a weak paramagnetic contribution is observed, likely due to the presence of an Yb$^{III}$ containing impurity. This behavior is in agreement with structural features observed for these systems, which point to an Yb$^{II}$-closed shell ligand electronic distribution. On the other hand, **3d** is characterized by a much more complex magnetic

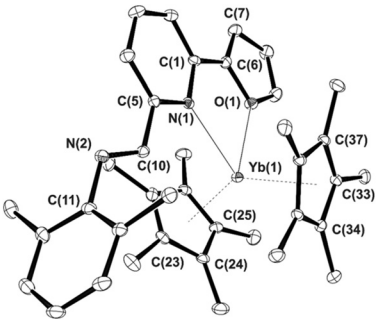


Fig. 4 ORTEP diagram (30% probability thermal ellipsoids) of complex ($C_5Me_5$)$_2$Yb[$\kappa^2$-2,6-$^i$Pr$_2$C$_6$H$_3$NCH(C$_5$H$_4$N)-6-(C$_4$H$_3$O)] (**3b**). Hydrogen atoms, Me-substituents of $^i$Pr-groups and one toluene molecule of crystallization are omitted for clarity. Selected bond distances (Å) and bond angles (°): Yb(1)–O(1) 2.468(2), Yb(1)–N(1) 2.535(2), Yb(1)–C(33) 2.676(2), Yb(1)–C(34) 2.678(2), Yb(1)–C(23) 2.679(3), Yb(1)–C(35) 2.687(2), Yb(1)–C(24) 2.690(3), Yb(1)–C(27) 2.692(3), Yb(1)–C(37) 2.694(2), Yb(1)–C(25) 2.695(3), Yb(1)–C(36) 2.697(2), Yb(1)–C(26) 2.709(2), N(2)–C(10) 1.264(3), C(5)–C(10) 1.475(4), O(1)–Yb(1)–N(1) 66.8(6).

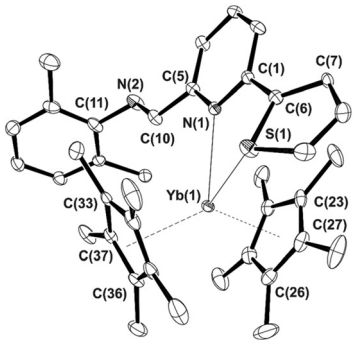


Fig. 5 ORTEP diagram (30% probability thermal ellipsoids) of complex ($C_5Me_5$)$_2$Yb[$\kappa^2$-2,6-$^i$Pr$_2$C$_6$H$_3$NCH(C$_5$H$_4$N)-6-(C$_4$H$_3$S)] (**3c**). Hydrogen atoms and Me-substituents of $^i$Pr-groups are omitted for clarity. Selected bond distances (Å) and bond angles (°): Yb(1)–N(1) 2.623(2), Yb(1)–S(1) 3.0103(7), Yb(1)–C(26) 2.645(3), Yb(1)–C(27) 2.669(3), Yb(1)–C(35) 2.696(3), Yb(1)–C(25) 2.699(3), Yb(1)–C(36) 2.712(2), Yb(1)–C(37) 2.723(3), Yb(1)–C(34) 2.730(3), Yb(1)–C(23) 2.732(3), Yb(1)–C(24) 2.741(3), Yb(1)–C(33) 2.764(3), N(2)–C(10) 1.258(4), C(5)–C(10) 1.468(4), N(1)–Yb(1)–S(1) 65.15(4).

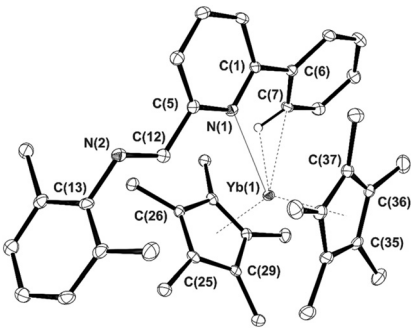


Fig. 6 ORTEP diagram (30% probability thermal ellipsoids) of complex ($C_5Me_5$)$_2$Yb[$\kappa^1$-2,6-$^i$Pr$_2$C$_6$H$_3$NCH(C$_5$H$_4$N)-6-Ph] (**3d**). Hydrogen atoms [except H(7)] and Me-substituents of $^i$Pr-groups are omitted for clarity. Selected bond distances (Å) and bond angles (°): Yb(1)–N(1) 2.602(2), Yb(1)–C(7) 2.969(3), Yb(1)–C(39) 2.683(3), Yb(1)–C(28) 2.683(2), Yb(1)–C(29) 2.692(2), Yb(1)–C(35) 2.695(3), Yb(1)–C(38) 2.702(3), Yb(1)–C(36) 2.712(2), Yb(1)–C(37) 2.718(2), Yb(1)–C(25) 2.736(2), Yb(1)–C(27) 2.758(2), Yb(1)–C(26) 2.776(2), C(5)–C(12) 1.488(4), N(1)–Yb(1)–C(7) 62.48(7).

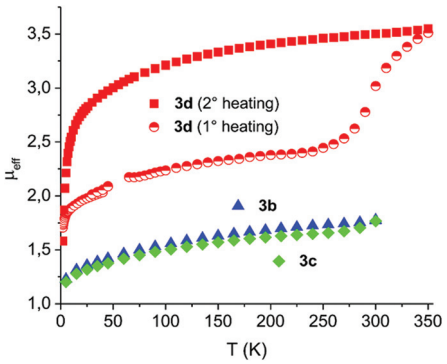


Fig. 7 $\mu_{eff}$ *vs. T* curve for **3b** (blue triangles), **3c** (green rhombus) and **3d**. For the latter, after the first heating cycle (red and white circles) the sample has been cooled down to 2 K and heated again up to 350 K (red squares).

behavior. It presents a $\mu_{eff}$ value of 2.4 up to 280 K that is much lower than that expected for a single $Yb^{III}$-species and a radical anionic ligand, even assuming them to be antiferromagnetically coupled. Such a $\mu_{eff}$ value is also completely different from that presumed for a diamagnetic $Yb^{II}$-closed shell system. On the other hand, no maximum in $\chi_M$ *vs. T*, which would be indicative of a multiconfigurational ground state, is observed (see Fig. S17 of the ESI†). Notably, heating **3d** from 270 K to 350 K gives rise to a clear-cut increase of the $\mu_{eff}$ value to 3.55. Such a variation is irreversible as witnessed by repeating the measurement after cooling down the sample. The value observed at high temperature is consistent with that expected for a strong antiferromagnetically coupled $Yb^{III}$-radical system, resulting in a $^1F_3$ state due to the combination of the $^2F_{7/2}$ term of $Yb^{III}$ and the $^2S_{1/2}$ term of a radical-anionic ligand.[40]

It is noteworthy that the $\mu_{eff}$ *vs. T* profile obtained after the first heating/cooling cycle can be perfectly rescaled, up to 270 K, on the pristine curve (see Fig. S18 of the ESI†). This result suggests that the species formed after heating above 270 K is also responsible for the intermediate $\mu_{eff}$ value measured before heating. Such a behavior can be reasonably explained by considering that the process leading to the increased $\mu_{eff}$ is already operative at room temperature (since the increase is visible above 270 K). Therefore, transformation already partially occurred when the sample is initially cooled down for measuring its magnetic properties. In other terms, the results of the magnetic investigation coupled with the outcomes of X-ray diffraction suggest that what we are actually measuring is not the structurally characterized form of **3d**, but rather a product which evolves from **3d** at $T > 270$ K. In this framework, it is tempting to attribute to **3d** a diamagnetic character and to the evolution product a $Yb^{III}$-radical one. However, in the absence of definitive clues or clear-cut experimental evidence, this is a purely speculative hypothesis. Finally, we wish to stress here that a simple redox isomeric transition involving **3d** cannot be invoked to explain the observed behaviour, since this should favour a closed shell configuration at high temperature.[41] However, if a structural rearrangement takes place on heating, this might favour the $Yb^{III}$-radical charge distribution; such a coupled structural/electronic transition would be in analogy to what is often observed in the case of $Co^{II}$ complexes presenting similar temperature dependence of magnetic moment.[19,42]

In contrast to **3a**, the $^1H$ NMR spectra of **3b–d** (benzene-$d_6$, 293 K) prove their diamagnetic nature in solution. The methyl protons of $C_5Me_5$ rings in **3b**, **3c** and **3d** appear as singlets at 1.92, 2.11 and 2.24 ppm respectively, and they are in line with the chemical shifts earlier reported for diamagnetic complexes $(C_5Me_5)_2Yb(L)_n$ with coordinated O-, N-, and P-containing Lewis bases.[43] At the same time, the signals of IPy ligands (**2b–d**) coordinated to the Yb ions in the $^1H$ NMR spectra give rise to the expected sets of signals with typical chemical shifts (see the ESI†). Finally, the UV-Vis spectra of **3b–d** are consistent with the diamagnetic nature of these complexes in solution.

Calculations were carried out in order to determine the electronic nature of complexes **3a,b,d**. The computational strategy is the same as that was developed by one of us (LM) to study multireference ground state complexes in bipyridine/phenanthroline Yb complexes.[39,40,44] In summary, first DFT (B3PW91) geometry optimization using small core Relativistic Effective Core Potentials (RECP) was carried out and in a second step CASSCF calculations were performed. For complex **3a**, within the precision of the DFT calculations, the displacement of a THF molecule from $Cp^*_2Yb(THF)$ by the ligand **2a** is expected to generate a $Yb^{III}$ complex through an exothermic process (3.8 kcal $mol^{-1}$) whereas the formation of a $Yb^{II}$ species is virtually thermoneutral (0.7 kcal $mol^{-1}$).[45] Due to this very small energy difference between the $Yb^{II}$ and $Yb^{III}$ complexes, CASSCF calculations were carried out. As in previous CASSCF calculations on ytterbium, different active spaces were used. A first one distributing 14 electrons into the 8 orbitals (the 7 4f of the Yb and the $\pi^*$ one of the ligand) was used and leads to similar results to the 8 electrons/5 orbitals (4 4f + $\pi^*$) one. Finally, a reduced active space of 4 electrons/3 orbitals (2 4f + $\pi^*$) was tested and gave the same qualitative results as the two others. Therefore, only the results obtained with the last one are discussed here for the sake of simplicity. Two singlet states, a closed shell one ($f^{14}$) and an open-shell one (multiconfigurational state $f^{14} + f^{13}$), and a triplet state were computed. The open-shell singlet state was found to be the ground state with the triplet state only 4.1 kcal $mol^{-1}$ higher in energy and the closed-shell singlet is 5.3 kcal $mol^{-1}$ higher in energy than the ground-state. The open-shell singlet state is formed by 78% of $Yb^{III}$ and 22% of $Yb^{II}$. This is in line with the magnetic measurement that indicates that complex **3a** is exhibiting a multiconfigurational character in the ground state with a major contribution from $Yb^{III}$.

In the same way, calculations were carried out on complex **3b**. Unlike complex **3a**, the coordination of the iminopyridine is not exothermic but rather slightly endothermic (5.8 kcal $mol^{-1}$). The formation of the $Yb^{III}$ complex from the $Yb^{II}$ one is also endothermic by up to 8.9 kcal $mol^{-1}$, making this highly unfavorable. To ensure this value, similar CASSCF calculations

 

were carried out and the closed-shell singlet [$Yb^{II}$] turned out to be the lowest by up to 10.6 kcal $mol^{-1}$ with respect to the triplet state (**3b**); the open-shell singlet being even higher in energy at 12.3 kcal $mol^{-1}$. This is again in line with the magnetic measurement that indicates that the ground state of **3b** is diamagnetic.

Finally, the calculations were conducted on the interesting **3d** complex. At the DFT level, the coordination of the iminopyridine is found to be even more endothermic (14.6 kcal $mol^{-1}$) and the formation of the $Yb^{III}$ complex is endothermic by 3.3 kcal $mol^{-1}$ from the $Yb^{II}$ one. Unlike the other cases, it is the coordination that appears to be complicated, it might not be the CASSCF calculations that would yield the answer. Indeed, at this level, the open-shell singlet is also found to be the ground state but with the triplet state almost degenerate (1.2 kcal $mol^{-1}$) and the closed-shell singlet only 5.3 kcal $mol^{-1}$ higher in energy. With such low energy differences between the states, it is hard to conclude on the nature of the ground state.

For a family of metallocene-type $Yb^{III}$ complexes coordinated by radical-anionic diazabutadiene ligands, the existence of a reversible solvent mediated ligand-to-metal electron transfer has been formerly discovered.[5c,6] This phenomenon consists of the displacement of the radical-anionic diazabutadiene ligand by molecules of a coordinating solvent (THF, DME, Py) followed by electron transfer from the diazabutadiene radical anion to the ytterbium ion: as a whole, the process results in the oxidation of the ligand to the neutral diazabutadiene and the reduction of $Yb^{III}$ to $Yb^{II}$ (Scheme 3).

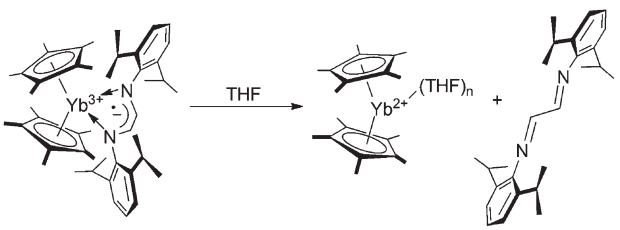


**Scheme 3** Solvent mediated ligand-to-metal electron transfer on a metallocene $Yb^{III}$ complex coordinated by a radical-anionic diazabutadiene ligand.

In order to check whether this behavior applies to related coordination compounds featuring IPy ligands, the reaction of **3a** with THF was carried out. Unlike diazabutadiene congeners, **3a** remains paramagnetic in THF-$d_8$ solution and no redox replacement of the iminopyridine ligand by THF occurs (Scheme 4). In contrast to **3a**, the addition of a stoichiometric amount of THF-$d_8$ to benzene-$d_6$ solutions of **3b–d** resulted in the immediate replacement of the IPy ligands in the Yb coordination sphere by THF. The $^1$H NMR spectra of **3b–d** recorded in THF-$d_8$/benzene-$d_6$ mixtures have unambiguously demonstrated the generation of $(C_5Me_5)_2Yb(THF)_n$ and free IPy ligands **2b–d** (Scheme 4). This result highlights the different reactivity of complexes **3b–d** from **3a** with respect to the replacement of IPy ligands by THF most likely caused by the different nature of metal–ligand interaction in these complexes. In addition, it demonstrates that metallocene type $Yb^{III}$ complexes coordinated by chelating radical-anionic diazabutadiene and IPy ligands behave differently in the presence of a coordinating solvent, despite their similar nature.

It can be inferred that such a different behavior between diazabutadienes and IPys is reasonably ascribed to the higher steric demand of the former class of ligands that is claimed to weaken the metal–ligand interaction. In **3a** the energy of formation for $Cp^*_2Yb^{II}$-THF is not sufficient to compensate for the energy loss for the cleavage of Coulombic interaction between the $Yb^{III}$ ion and the radical-anionic iminopyridine ligand. At the same time, the quick IPy displacement by stoichiometric amounts of THF in complexes **3b–d** coordinated by a neutral IPy ligand is in line with the energies of coordination bonds in $Yb^{II}$ complexes with N- and O-containing ligands.

## Conclusions

In this paper we have described a new example of sterically controlled metal–ligand electron transfer by reacting $(C_5Me_5)_2Yb(THF)$ with IPy ligands featuring very similar electron accepting properties but variable denticity and steric

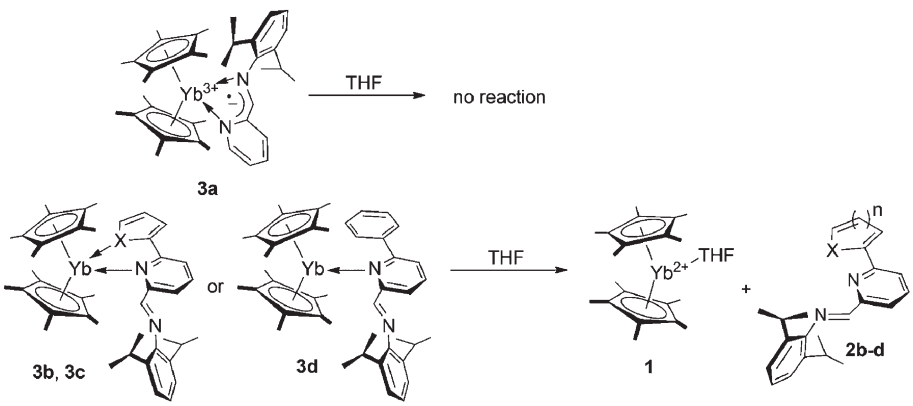


**Scheme 4** Solvent mediated ligand-to-metal electron transfer on coordination compounds **3a–d**.

demand. The reactions of $(C_5Me_5)_2Yb(THF)$ with ligands **2a–d** proceed with the displacement of the coordinated THF molecule by means of an IPy framework. The observed outcomes highlight an important effect related to the steric demand of the iminopyridine systems on both their coordination mode and on their ability to foster metal-to-ligand electron transfer phenomena. Thus, the less sterically crowded **2a** coordinates the metal ion as a bidentate system and a metal-to-ligand electron transfer takes place with the formation of a trivalent ytterbium species coordinated by a radical anionic IPy ligand. With the bulkier **2b** and **2c**, potentially featuring as tridentate systems, the coordination to the metal ions takes place through the pyridine nitrogen and either O or S atoms of the heteroaryl substituents, only. For these neutral coordinative $Yb^{II}$-complexes (**3b** and **3c**) the imine nitrogen points away from the metal coordination sphere. For the bidentate **2d** ligand, featuring steric hindrance similar to **2b–c**, a monodentate coordination to the $Yb^{II}$ ion is accomplished through the pyridine nitrogen only. The reason which blocks metal-to-ligand electron transfer in compounds **2b–d** is likely the impossibility of a close approach between the ytterbium center and the bulkier substituted IPy ligands as a consequence of a metal ion size decrease in the case of a $Yb^{II}/Yb^{III}$ oxidation. We note that while this trend is clearly defined in solution by NMR and in the solid state by X-ray data, magnetic analysis in the solid state confirms it only for **3a–c**. The former complex provides a magnetic response that is as expected for a multiconfigurational ground state with the largest contribution from the $4f^{13}$-radical configuration, while **3b** and **3c** are diamagnetic and thus consistent with the closed-shell singlet ground state configuration. On the contrary, the magnetic behavior of **3d** turned out to be extremely complex, suggesting the instability of its structure on heating above 270 K.

Unlike indenyl ligands cyclopentadienyl analogues are not prone to haptotropic rearrangements and the use of $Cp^*_2Yb(THF)$ provided us with an opportunity to demonstrate clearly and unambiguously that bulkiness and the electronic properties of the aromatic carbocyclic ligands coordinated to the $Yb^{II}$ ion are also decisive for the occurrence of intramolecular metal-to-ligand electron transfer and the type of coordination adopted by IPy ligands. The bidentate coordination of less sterically demanding Ipy **2a** allows for a metal-to-ligand electron transfer resulting in a shortening of the Yb–Cp* bonds and the formation of rather short Yb–N bonds (Yb(1)–N(1) 2.325(2) Å). The introduction of bulky substituents into the Py ring excludes the possibility of such structural changes associated with oxidation and blocks the metal-to-ligand electron transfer. Indeed the resulting IPy complexes **2b–d** feature Yb–Cp* and Yb–N distances characteristic for $Yb^{II}$ species.

## Conflicts of interest

There are no conflicts to declare.

## Acknowledgements

This work was financially supported by the Russian Science Foundation (Project 17-73-30036).

## References

1 (*a*) F. G. N. Cloke, H. C. de Lemos and A. A. Sameh, *J. Chem. Soc., Chem. Commun.*, 1986, 1344–1345; (*b*) F. G. N. Cloke, *Chem. Soc. Rev.*, 1993, **22**, 17–21; (*c*) A. Recknagel, M. Noltemeyer and F. T. Edelmann, *J. Organomet. Chem.*, 1991, **410**, 53–61; (*d*) P. Poremba and F. T. Edelmann, *J. Organomet. Chem.*, 1997, **549**, 101–104.

2 (*a*) T. V. Mahrova, G. K. Fukin, A. V. Cherkasov, A. A. Trifonov, N. Ajellal and J.-F. Carpentier, *Inorg. Chem.*, 2009, **48**, 4258–4266; (*b*) H. Kaneko, H. Nagae, H. Tsurugi and K. Mashima, *J. Am. Chem. Soc.*, 2011, **133**, 19626–19629; (*c*) A. A. Kissel, D. M. Lyubov, T. V. Mahrova, G. K. Fukin, A. V. Cherkasov, T. A. Glukhova, D. Cui and A. A. Trifonov, *Dalton Trans.*, 2013, **42**, 9211–9225; (*d*) H. Kaneko, H. Tsurugi, T. K. Panda and K. Mashima, *Organometallics*, 2010, **29**, 3463–3466; (*e*) K.-H. Thiele, V. Lorenz, G. Thiele, P. Zoennchen and J. Scholz, *Angew. Chem., Int. Ed. Engl.*, 1994, **33**, 1372–1373; (*f*) H. Görls, B. Neumüller, A. Scholz and J. Scholz, *Angew. Chem., Int. Ed. Engl.*, 1995, **34**, 673–676; (*g*) A. A. Kissel, T. V. Mahrova, D. M. Lyubov, A. V. Cherkasov, G. K. Fukin, A. A. Trifonov, I. Del Rosal and L. Maron, *Dalton Trans.*, 2015, **44**, 12137–12148.

3 (*a*) H. tom Dieck and I. W. Renk, *Chem. Ber.*, 1971, **104**, 110–130; (*b*) H. tom Dieck, K.-D. Franz and F. Hoffmann, *Chem. Ber.*, 1975, **108**, 163–173; (*c*) J. Reinhold, R. Benedix, P. Birner and H. Hennig, *Inorg. Chem.*, 1979, **33**, 209–213.

4 (*a*) L. R. Morss, *Chem. Rev.*, 1976, **76**, 827–841; (*b*) R. G. Finke, S. R. Keenan, D. A. Shirardi and P. L. Watson, *Organometallics*, 1986, **5**, 598–601; (*c*) A. M. Bond, G. B. Deacon and R. H. Newnham, *Organometallics*, 1986, **5**, 2312–2316.

5 (*a*) A. A. Trifonov, *Eur. J. Inorg. Chem.*, 2007, 3151–3167; (*b*) M. D. Walter, D. J. Berg and R. A. Andersen, *Organometallics*, 2007, **26**, 2296–2307; (*c*) P. Cui, Y. Chen, G. Wang, G. Li and W. Xia, *Organometallics*, 2008, **27**, 4013–4016; (*d*) K. Vasudevan and A. H. Cowley, *Chem. Commun.*, 2007, 3464–3466.

6 (*a*) A. A. Trifonov, Yu. A. Kurskii, M. N. Bochkarev, S. Muehle, S. Dechert and H. Schumann, *Russ. Chem. Bull.*, 2003, **52**, 601–606; (*b*) A. A. Trifonov, E. A. Fedorova, G. K. Fukin, V. N. Ikorskii, Yu. A. Kurskii, S. Dechert, H. Schumann and M. N. Bochkarev, *Russ. Chem. Bull.*, 2004, **53**, 2736–2743; (*c*) A. A. Trifonov, E. A. Fedorova, V. N. Ikorskii, S. Dechert, H. Schumann and M. N. Bochkarev, *Eur. J. Inorg. Chem.*, 2005, 2812–2818.

7 A. A. Trifonov, I. A. Borovkov, E. A. Fedorova, G. K. Fukin, J. Larionova, N. O. Druzhkov and V. K. Cherkasov, *Chem. – Eur. J.*, 2007, **13**, 4981–4987.

 

8 I. L. Fedushkin, O. V. Maslova, A. G. Morozov, S. Dechert, S. Demeshko and F. Meyer, *Angew. Chem., Int. Ed.*, 2012, **51**, 10584–10587.
9 I. D. Gridnev, *Coord. Chem. Rev.*, 2008, **252**, 1798–1818.
10 A. A. Trifonov, E. N. Kirillov, M. N. Bochkarev, H. Schumann and S. Muehle, *Russ. Chem. Bull.*, 1999, **48**, 382–384.
11 (*a*) A. A. Trifonov, E. A. Fedorova, G. K. Fukin, N. O. Druzhkov and M. N. Bochkarev, *Angew. Chem., Int. Ed.*, 2004, **43**, 5045–5048; (*b*) A. A. Trifonov, E. A. Fedorova, I. A. Borovkov, G. K. Fukin, E. V. Baranov, J. Larionova and N. O. Druzhkov, *Organometallics*, 2007, **26**, 2488–2491.
12 A. A. Trifonov, E. A. Fedorova, G. K. Fukin, E. V. Baranov, N. O. Druzhkov and M. N. Bochkarev, *Chem. – Eur. J.*, 2006, **12**, 2752–2757.
13 A. A. Trifonov, B. G. Shestakov, K. A. Lyssenko, J. Larionova, G. K. Fukin and A. V. Cherkasov, *Organometallics*, 2011, **30**, 4882–4889.
14 G. Giambastiani and J. Campora, in *Olefin Upgrading Catalysis by Nitrogen-based Metal Complexes, I and II*, Springer, London, 2011, p. 287 and 265.
15 A. A. Trifonov, I. D. Gudilenkov, J. Larionova, C. Luna, G. K. Fukin, A. V. Cherkasov, A. I. Poddel'sky and N. O. Druzhkov, *Organometallics*, 2009, **28**, 6707–6713.
16 A. A. Trifonov, B. G. Shestakov, I. D. Gudilenkov, G. K. Fukin, G. Giambastiani, C. Bianchini, A. Rossin, L. Luconi, J. Filippi and L. Sorace, *Dalton Trans.*, 2011, **40**, 10568–10575.
17 R. D. Shannon, *Acta Crystallogr., Sect. A: Cryst. Phys., Diffr., Theor. Gen. Crystallogr.*, 1976, **32**, 751–767.
18 T. Don Tilley, R. A. Andersen, B. Spencer, H. Ruben, A. Zalkin and D. H. Templeton, *Inorg. Chem.*, 1980, **19**, 2999–3003.
19 Z. Benko, S. Burck, D. Gudat, M. Nieger, L. Nyulaszi and N. Shore, *Dalton Trans.*, 2008, 4937–4945.
20 (*a*) C. Bianchini, G. Giambastiani, G. Mantovani, A. Meli and D. Mimeau, *J. Organomet. Chem.*, 2004, **689**, 1356–1361; (*b*) C. Bianchini, D. Gatteschi, G. Giambastiani, I. Guerrero Rios, A. Ienco, F. Laschi, C. Mealli, A. Meli, L. Sorace, A. Toti and F. Vizza, *Organometallics*, 2007, **26**, 726–739; (*c*) C. Bianchini, G. Mantovani, A. Meli, F. Migliacci and F. Laschi, *Organometallics*, 2003, **22**, 2545–2547.
21 S. J. Lyle and M. M. Rahman, *Talanta*, 1953, **10**, 1177–1182.
22 M. Bruker, *SMART*, Bruker AXS Inc., Wisconsin, USA, 2012.
23 M. Bruker, *APEX2*, Bruker AXS Inc., Wisconsin, USA, 2012.
24 Y. Agilent, *CrysAlis PRO*, Agilent Technologies Ltd, Oxfordshire, England, 2014.
25 (*a*) G. M. Sheldrick, *Acta Crystallogr., Sect. A: Found. Adv.*, 2015, **71**, 3–8; (*b*) G. M. Sheldrick, *Acta Crystallogr., Sect. C: Struct. Chem.*, 2015, **71**, 3–8.
26 M. Bruker, *SADABS*, Bruker AXS Inc., Wisconsin, USA, 2001.
27 M. J. Frisch, G. W. Trucks, H. B. Schlegel, G. E. Scuseria, M. A. Robb, J. R. Cheeseman, G. Scalmani, V. Barone, B. Mennucci, G. A. Petersson, H. Nakatsuji, M. Caricato, X. Li, H. P. Hratchian, A. F. Izmaylov, J. Bloino, G. Zheng, J. L. Sonnenberg, M. Hada, M. Ehara, K. Toyota, R. Fukuda, J. Hasegawa, M. Ishida, T. Nakajima, Y. Honda, O. Kitao, H. Nakai, T. Vreven, J. A. Montgomery, Jr., J. E. Peralta, F. Ogliaro, M. Bearpark, J. J. Heyd, E. Brothers, K. N. Kudin, V. N. Staroverov, R. Kobayashi, J. Normand, K. Raghavachari, A. Rendell, J. C. Burant, S. S. Iyengar, J. Tomasi, M. Cossi, N. Rega, J. M. Millam, M. Klene, J. E. Knox, J. B. Cross, V. Bakken, C. Adamo, J. Jaramillo, R. Gomperts, R. E. Stratmann, O. Yazyev, A. J. Austin, R. Cammi, C. Pomelli, J. W. Ochterski, R. L. Martin, K. Morokuma, V. G. Zakrzewski, G. A. Voth, P. Salvador, J. J. Dannenberg, S. Dapprich, A. D. Daniels, Ö. Farkas, J. B. Foresman, J. V. Ortiz, J. Cioslowski and D. J. Fox, *Gaussian 09*, Gaussian Inc., Wallingford CT, 2009.
28 (*a*) A. D. Becke, *J. Chem. Phys.*, 1993, **98**, 5648–5652; (*b*) J. P. Perdew and Y. Wang, *Phys. Rev. B: Condens. Matter Mater. Phys.*, 1992, **45**, 13244–13249; (*c*) J. P. Perdew, Y. Wand and Y. K. Burke, in *Electronic Density Functional Theory: Recent Progress and New Directions*, ed. J. F. Dobson, G. Vignale and M. P. Das, Plenum, New York, 1998.
29 (*a*) M. Dolg, A. Stoll, A. Savin and H. Preuss, *Theor. Chim. Acta*, 1989, **75**, 173–194; (*b*) M. Dolg, H. Stoll and H. Rreuss, *Theor. Chim. Acta*, 1993, **85**, 441–450.
30 P. C. Hariharan and J. A. Pople, *Theor. Chim. Acta*, 1973, **28**, 213–222.
31 M. Schultz, C. J. Burns, D. J. Schwartz and R. A. Andersen, *Organometallics*, 2000, **19**, 781–789.
32 T. Don Tilley, R. A. Andersen, B. Spencer and A. Zalkin, *Inorg. Chem.*, 1982, **21**, 2647–2649.
33 I. A. Borovkov, G. K. Fukin and A. A. Trifonov, *Russ. Chem. Bull.*, 2008, **57**, 541–545.
34 G. Zi, Q. Yang, T. C. W. Mak and Z. Xie, *Organometallics*, 2001, **20**, 2359–2366.
35 P. L. Watson, T. H. Tulip and I. Williams, *Organometallics*, 1990, **9**, 1999–2009.
36 (*a*) V. C. Gibson, R. K. O'Reily, D. F. Wass, A. J. P. White and D. J. Williams, *Dalton Trans.*, 2003, 2824–2830; (*b*) T. V. Laine, M. Klinga and M. Leskelä, *Eur. J. Inorg. Chem.*, 1999, 959–964; (*c*) T. V. Laine, U. Piironen, K. Lappalainen, M. Klinga, E. Aitolla and M. Leskelä, *J. Organomet. Chem.*, 2000, **606**, 112–124.
37 (*a*) C. C. Lu, E. Bill, T. Weyhermüller, E. Bothe and K. Wieghardt, *J. Am. Chem. Soc.*, 2008, **130**, 3181–3197; (*b*) C. C. Lu, G. S. De Beer, T. Weyhermüller, E. Bill, E. Bothe and K. Wieghardt, *Angew. Chem., Int. Ed.*, 2008, **47**, 6384–6387; (*c*) O. T. Summerscales, T. W. Myers and L. A. Berben, *Organometallics*, 2012, **31**, 3463–3465.
38 A. Abragam and B. Bleaney, *Electron paramagnetic resonance of transitionions*, Oxford University Press, Oxford, England, 1970.
39 C. H. Booth, M. D. Walter, D. Kazhdan, Y.-J. Hu, W. W. Lukens, E. D. Bauer, L. Maron, O. Eisenstein and R. A. Andersen, *J. Am. Chem. Soc.*, 2009, **131**, 6480–6491.
40 M. Schultz, J. M. Boncella, D. J. Berg, T. Don Tilley and R. A. Andersen, *Organometallics*, 2002, **21**, 460–472.

41 I. L. Fedushkin, O. V. Maslova, E. V. Baranov and A. S. Shavyrin, *Inorg. Chem.*, 2009, **48**, 2355–2357.
42 (*a*) K. G. Alley, G. Poneti, P. S. D. Robinson, A. Nafady, B. Moubaraki, J. B. Aitken, S. C. Drew, C. Ritchie, B. F. Abrahams, R. K. Hocking, K. S. Murray, A. M. Bond, H. H. Harris, L. Sorace and C. Boskovic, *J. Am. Chem. Soc.*, 2013, **135**, 8304–8323; (*b*) O. Drath, R. W. Gable, B. Moubaraki, K. S. Murray, G. Poneti, L. Sorace and C. Boskovic, *Inorg. Chem.*, 2016, **55**, 4141–4151.
43 (*a*) A. G. Avent, M. A. Edelman, M. F. Lappert and G. A. Lawless, *J. Am. Chem. Soc.*, 1989, **111**, 3423–3425; (*b*) D. J. Schwartz and R. A. Andersen, *Organometallics*, 1995, **14**, 4308–4318.
44 (*a*) G. Nocton, C. H. Booth, L. Maron and R. A. Andersen, *Organometallics*, 2013, **32**, 1150–1158; (*b*) G. Nocton, C. H. Booth, L. Maron and R. A. Andersen, *Organometallics*, 2013, **32**, 5305–5312; (*c*) C. H. Booth, D. Kazhdan, E. L. Werkema, M. D. Walter, W. W. Lukens, E. D. Bauer, Y.-J. Hu, L. Maron, O. Eisenstein, M. Head-Gordon and R. A. Andersen, *J. Am. Chem. Soc.*, 2010, **132**, 17537–17549; (*d*) G. Nocton, C. H. Booth, L. Maron, L. Ricard and R. A. Andersen, *Organometallics*, 2014, **33**, 6819–6829; (*e*) G. Nocton, W. W. Lukens, C. H. Booth, S. S. Rozenel, S. A. Medling, L. Maron and R. A. Andersen, *J. Am. Chem. Soc.*, 2014, **136**, 8626–8641; (*f*) M. D. Walter, D. J. Berg and R. A. Andersen, *Organometallics*, 2006, **25**, 3228–3237.
45 (*a*) Y. Zhao and D. G. Truhlar, *Acc. Chem. Res.*, 2008, **41**, 157–167; (*b*) N. E. Schultz, Y. Zhao and D. G. Truhlar, *J. Comput. Chem.*, 2008, **29**, 185–189.